250-GHz Electron Spin Resonance Studies of Polarity Gradients Along the Aliphatic Chains in Phospholipid Membranes

Keith A. Earle, Jozef K. Moscicki, Mingtao Ge, David E. Budil, and Jack H. Freed
Baker Laboratory of Chemistry, Cornell University, Ithaca, New York 14853 USA

ABSTRACT Rigid-limit 250-GHz electron spin resonance (FIR-ESR) spectra have been studied for a series of phosphatidylcholine spin labels (*n*-PC, where $n = 5, 7, 10, 12, 16$) in pure lipid dispersions of dipalmitoylphosphatidylcholine (DPPC) and 1-palmitoyl-2-oleoylphosphatidylcholine (POPC), as well as dispersions of DPPC containing the peptide gramicidin A (GA) in a 1:1 molar ratio. The enhanced *g*-tensor resolution of 250-GHz ESR for these spin labels permitted a careful study of the nitroxide *g*-tensor as a function of spin probe location and membrane composition. In particular, as the spin label is displaced from the polar head group, A_{zz} decreases and g_{xx} increases as they assume values typical of a nonpolar environment, appropriate for the hydrophobic alkyl chains in the case of pure lipid dispersions. The field shifts of spectral features due to changes in g_{xx} are an order of magnitude larger than those from changes in A_{zz}. The magnetic tensor parameters measured in the presence of GA were characteristic of a polar environment and showed only a very weak dependence of A_{zz} and g_{xx} on label position. These results demonstrate the significant influence of GA on the local polarity along the lipid molecule, and may reflect increased penetration of water into the alkyl chain region of the lipid in the presence of GA. The spectra from the pure lipid dispersions also exhibit a broad background signal that is most significant for 7-, 10-, and 12-PC, and is more pronounced in DPPC than in POPC. It is attributed to spin probe aggregation yielding spin exchange narrowing. The addition of GA to DPPC essentially suppressed the broad background signal observed in pure DPPC dispersions.

INTRODUCTION

Electron paramagnetic resonance (EPR) studies of nitroxide spin labels have been an important tool for investigating structure and dynamics in a wide variety of membrane systems (Hyde et al., 1979; Jost and Griffith, 1982; Marsh, 1985; Marsh, 1989; Ge and Freed, 1993). Successful application of such methods depends in large part on the accuracy and precision with which the magnetic parameters of the nitroxyl radical probe can be measured. The extension of EPR methods to high frequencies requiring superconducting magnets (Grinberg et al., 1983; Ondar et al., 1985a; Burghaus et al., 1988; Lynch et al., 1988; Budil et al., 1989; Muller et al., 1989; Prisner et al., 1992) has significantly improved the resolution of rigid-limit spectra from which the *g*-tensor, as well as the nitrogen nuclear hyperfine interaction tensor (*A*), can be determined for nitroxides. This advance, in turn, has enhanced the overall reliability of the spin-label method.

In addition to providing accurate magnetic tensors as a basis for investigations of spin-label dynamics, high-frequency EPR significantly improves the sensitivity to local structural influences on the spin label, even without isotopic labeling. Specifically, the polarity of the "microenvironment" in which the nitroxide moiety finds itself has a strong effect on both the *g*- and *A*-tensors, most notably the measured values of g_{xx} and A_{zz}. Extensive investigations by Lebedev and co-workers at 140 GHz (Krinichnyi et al., 1985; Ondar et al., 1985a,b) have revealed small but significant changes in the *g*-tensor as a function of solvent polarity and chemical structure of the nitroxide. They also demonstrated a high degree of correlation between g_{xx} and A_{zz} as a function of solvent polarity, consistent with earlier work (Kawamura et al., 1967). These results suggest that nitroxide spin labels may be quite useful as probes of local polarity at different positions within the membrane bilayer. A previous study of polarity gradients (Griffith et al., 1974) has shown that rigid-limit tensor parameters can be a useful probe of membrane composition. That study was performed at 35 GHz, however, which is sensitive to the A_{zz} hyperfine tensor component but not to the detailed behavior of the *g*-tensor. Griffith et al. (1974) determined that there was indeed a polarity gradient that must be due to the nature of the lipid bilayer, because the variation in A_{zz} along the membrane bilayer that they observed with the PC spin labels they used was absent for the same spin-label series dissolved in homogeneous solvents of varying polarity.

The initial objective for the present work was to utilize the high spectral resolution at 250 GHz to refine previous estimates of the *g*- and *A*-tensors for different nitroxide spin probes in a range of membrane compositions. There were two basic motivations for this goal: first, accurate magnetic tensor values are an important prerequisite for quantitative studies of lipid dynamics and ordering (Kar et al., 1984; Tanaka and Freed, 1985; Shin and Freed, 1989; Ge and Freed, 1993); and second, a careful study of variations in the magnetic tensors might be expected to shed new light on detailed structural effects in the membrane by virtue of their sensitivity to polarity effects. Our initial efforts, reported here, give us confidence that we can exploit the enhanced sensitivity of FIR-ESR to slight variations in the polar environment of the spin probe to monitor changes in the extent

Received for publication 11 November 1993 and in final form 27 December 1993.

Dr. Moscicki is on sabbatical leave from the Institute of Physics of the Jagiellonian University, Reymonta 4, Cracow, Poland.

0006-3495/94/04/1213/09 $2.00

of water penetration into the hydrophobic lipid bilayer as a function of temperature, as has been explored for labeled lysosymes at different water contents (Krinichnyi et al., 1985). At conventional EPR frequencies such changes are difficult to observe, due to the limited resolution of the g-tensor.

Recent work from this laboratory (Ge and Freed, 1993) has shown that the addition of GA to membrane dispersions does have significant effects on rigid limit spectra from n-PC spin probes obtained at X-band, where the A-tensor dominates the spectral width. In particular, the addition of GA increases the resolution of the spectrum and also changes the observed A_{zz} values. At 250 GHz it has been possible to exploit the enhanced magnetic tensor resolution to observe not only changes in A_{zz} but also in g_{xx} when GA is added to the membrane. Indeed, we find that the changes in g_{xx} and A_{zz} lead to field shifts in the spectral features that are an order of magnitude larger for changes in g_{xx} than for changes in A_{zz}.

In addition to the typical EPR powder patterns from which accurate g- and A-tensors could be obtained, an additional feature appeared in the rigid-limit 250-GHz EPR spectra of many of the systems studied. Specifically, a striking broad background component appeared in 250-GHz EPR spectra of pure DPPC dispersions that was essentially absent in GA-containing dispersions of DPPC. The intensity and shape of the background signal was correlated closely with the chain position at which the doxyl nitroxide moiety was attached.

We note that doxyl spin labels induce a kink in the alkyl chain of n-PC spin probes (Broido et al., 1982), which may cause appreciable steric strains on the spin probes 7-, 10-, and 12-PC in the saturated lipid DPPC. Such strains may be correlated with an unusual dependence of g_{xx} and A_{zz} on chain position, a point which we address below. Thus the sensitivity of g_{xx} and A_{zz} to microenvironmental effects can also be invoked to study packing effects.

To estimate to what extent the background is associated with the steric incompatibility between hydrocarbon chains, we performed additional studies of n-PC/POPC dispersions. POPC has a kink at the C_9 position of the sn-2 chain due to an unsaturated bond, and is therefore sterically more similar to the n-PC spin labels than DPPC. Although the spectra from n-PC/POPC samples do exhibit a background signal qualitatively similar to that observed in n-PC/DPPC samples, there are some significant differences that suggest the spectrum does depend on the mixing interactions between spin label and host lipid. Our results suggest that the enhanced sensitivity of 250-GHz EPR to orientation of the nitroxide may offer a new means of probing mixing and clustering interactions in membrane systems via the spectral averaging effects of spin-spin interactions such as Heisenberg spin exchange (HE) and electron-electron dipolar (EED) couplings.

We note that the combined effects of having EPR powder patterns that are rather broad, as well as the background exchange narrowed signal in these membrane dispersions, lead to 9-GHz spectra with very limited resolution, but it is still not difficult to extract the magnetic tensors from the 250-GHz EPR spectra because of the significantly enhanced g-resolution. This challenge to spectral fitting is also discussed under Results.

EXPERIMENTAL METHODS

The spin probes and lipids used in this study were obtained from Avanti Polar Lipids (Birmingham, AL) and the GA was obtained from Sigma Chemical Co. (St. Louis, MO). All materials were used without further purification. Weighed amounts of lipid and GA, when desired, were dissolved in chloroform and methanol, respectively, and mixed together. Spin labels were added from stock solutions in chloroform to give concentrations of 1.0 mol % of the mixture, except for one 0.5 mol % sample of 10-PC/POPC that we prepared to study concentration effects. After the solution was thoroughly mixed, the solvent was evaporated by nitrogen gas flow and was completely removed by pumping on the sample overnight in a vacuum desiccator. The dried powder sample was deposited on a watch glass and placed in a humidifier. The samples were hydrated in a humid atmosphere at 25°C (in the gel phase) for at least 24 h before use to ensure that the samples had equilibrated. Water content in the samples was determined by weighing before and after drying them in an oven. The GA-free samples had a water content of approximately 20%, whereas those containing GA had a water content of approximately 10%. Both cases correspond to an isopotential of the chemical potential of water in the membrane and bulk water phases of the sample. After hydration, the resulting waxy substance was pressed into a pellet of approximately 8-mm diameter and 0.5- to 1.0-mm thickness depending on the amount of water present to produce the samples for 250-GHz ESR. Higher water contents required somewhat thinner samples to avoid significant dielectric losses in the sample cavity. For 9-GHz ESR, the hydrated samples were placed in 1-mm-outside diameter pyrex tubes.

The home-built 250-GHz EPR spectrometer used in these experiments has been described previously (Budil et al., 1989). The spectrometer operates at a single fixed frequency, which is stabilized by phase locking to a 100-MHz, oven-controlled crystal oscillator (Vectron CO224A59XL2) through a frequency multiplier chain. Utilizing an HP8566B spectrum analyzer, the stabilized frequency of the Gunn (RF) oscillator was measured to be $83.300000 \pm 3 \times 10^{-5}$ GHz. When frequency tripled, this yielded a frequency of $249.90000 \pm 9 \times 10^{-5}$ GHz, i.e., a frequency stable to approximately 3 parts in 10^7. The magnetic field homogeneity is 1.5 parts in 10^6 across a 1-cm radius, and was verified using a ^{2}H nuclear magnetic resonance gaussmeter (Sentec model 1101). The magnetic field sweep was calibrated using a Mn^{2+}/MgO EPR standard as well as the gaussmeter. The absolute field values are known to three parts in 10^5 due to small uncertainties in the sweep calibration. The use of an internal standard with a g value known to at least six-part accuracy would enable absolute measurements of field positions to six-place accuracy. But the relative error, i.e., the error in a field position relative to a calibration point in the spectrum, may be taken as 1.5 parts in 10^6. The relative error in g values resulting from the spectral fits is somewhat higher than this (cf. Budil et al. (1993) and Results section (this work)).

To achieve stable control over the sample temperature, we incorporated a nitrogen flow channel into the bottom (flat) copper mirror of the semi-confocal Fabry-Perot resonator. The sample had a weak thermal link to the bottom mirror via the teflon sample holder, which made it necessary to monitor the temperature of the sample as well as the bottom mirror. The sample holder, which has been described previously (Budil et al., 1989), was modified to house a copper-constantan thermocouple near the sample, but away from the FIR active region of the resonator. The loose thermal contact between the bottom mirror and the sample also provided a measure of isolation from sudden temperature shifts caused by "breathing" of the liquid nitrogen storage dewar that we used for cooling. We were able to control the temperature of the sample to within ±0.5 K with this method. All rigid limit spectra were recorded at approximately −150°C.

Spectra were obtained using standard field modulation and lock-in detection with a time constant of 3 s, typically. The modulation amplitude was controlled by a locally designed and constructed solid-state transconductance amplifier (Autocratic Amplifier Associates, Intermod, NY) which was

optimized for driving inductive loads. For this work we used a modulation frequency of 47 kHz or 70 kHz depending on experimental convenience; however, the choice of modulation frequency did not have a significant effect on the signal-to-noise ratio. We also took care to ensure that the modulation amplitude was sufficiently low so that no distortion of the lineshape occurred, although this was hardly an issue for some of the very broad spectra that we observed.

When necessary, multiple scans were averaged to improve the signal-to-noise ratio; the spectra shown below typically represent 1–5 field scans. The spectra often exhibit a small admixture of a dispersion signal that can vary across the spectrum. The apparent phase of the spectrum depends on detector orientation as well as rotation of the plane-polarized mm-waves incident upon the sample, which depends in turn on sample dichroism (which can be field-dependent), and cavity tune. The methods used to recover a pure absorption signal have been discussed elsewhere (Earle et al., 1993). It is interesting to note, however, that the variation of the dispersion admixture across the spectrum was found to be partially suppressed on averaging multiple scans, as one might expect for a partially random process. Changes in cavity tune and detector alignment due to thermal fluctuations during repeated scans could easily account for the suppression effect that we observed.

After correction for phase variations, the spectra were analyzed using a modified Levenberg-Marquardt nonlinear least squares algorithm (Moré et al., 1980) combined with a slow-motional spectral calculation program based on the stochastic Liouville equation (Schneider and Freed, 1989). Satisfactory powder-pattern spectra could be obtained from the program by using rotational diffusion rates equivalent to the rigid limit, approximately $5 \times 10^5\ s^{-1}$. To extract the magnetic tensor parameters of the spin probes from the spectra, the difference between a calculated rigid-limit spectrum and the data was first minimized with respect to the magnetic tensor parameters. Once this was accomplished, a second "site" was added to the fitting procedure to model the broad background feature. The relative contributions of each "site" were determined by linear least squares at each iteration of the nonlinear least squares procedure (Golub and Pereyra, 1973). Both "sites" were assumed to have the same magnetic tensors, and the result of the single-site minimization was used to seed this second stage of minimization. To model the spectral averaging evident in the features of the second "site," we used an extension of our previous expressions for HE appropriate for orientational averaging at slow exchange rates (Freed, 1993). It should be noted that for the range of exchange rates that best fit the broad background, the simulations based on HE narrowing are almost indistinguishable from strong jump diffusion, although the underlying physical assumptions that go into jump diffusion are different from the HE case.

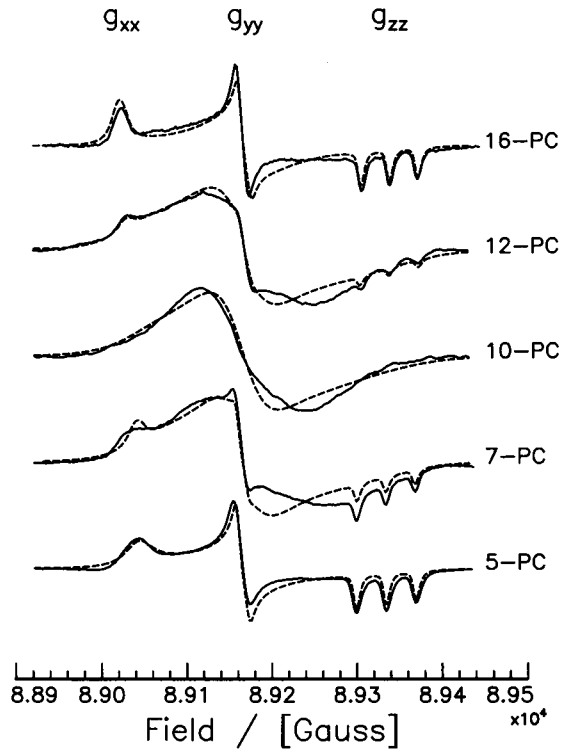

FIGURE 1 Rigid limit 250-GHz spectra of 5-, 7-, 10-, 12-, and 16-PC in pure DPPC (hydrated). The spectra are ordered from bottom to top: 5-, 7-, 10-, 12-, and 16-PC. Simulations of the spectra are shown by dotted lines for 5-, 7-, 12-, and 16-PC. It was not possible to determine rigid limit tensor parameters for 10-PC/DPPC for reasons discussed in the text. The magnetic tensor parameters derived from the fits are given in Table 1. We also indicate the regions of the rigid limit spectra corresponding to g_{xx}, g_{yy}, and g_{zz} by labels above the appropriate field values.

RESULTS

Figs. 1, 2, and 3 show rigid-limit 250-GHz spectra of the *n*-PC spin probes in dispersions of DPPC, DPPC:GA in a 1:1 molar ratio, and POPC, respectively. Most of the spectra exhibit a component corresponding to the typical nitroxide "powder pattern" lineshape expected for a dilute frozen solution of a nitroxide spin probe at 250 GHz (Budil et al., 1989). The spectral features of this component are clearly resolved into three separate regions corresponding to the *x*, *y*, and *z* "turning points" of the *g*-tensor, as indicated by labels above the relevant spectral features in Fig. 1.

In most of the spectra obtained from DPPC and POPC dispersions (cf. Figs. 1 and 3) a second broad background signal appears as noted above. The lineshape and intensity of this component depends strongly on the label position. In DPPC, for example, the spectrum of 10-PC consists entirely of the broad component, and the spectrum also exhibits the highest degree of spectral averaging in this case. For spin probes labeled at either end of the lipid chain (5-PC and 16-PC) the broad component is much less prominent in comparison with the rigid limit spectrum, and somewhat broader (i.e., exhibits less dynamic averaging) than that in 10-PC. The 7-PC and 12-PC probes exhibit features intermediate to these two extreme cases. Finally, we note that the broad feature did not change on reducing the spin probe concentration by a factor of 2 (cf. Fig. 4).

Surprisingly, we find that the addition of GA to the DPPC dispersion almost completely abolishes the broad background signal. This is clearly demonstrated in Fig. 2, where all the spectra closely resemble the calculated rigid-limit powder pattern (shown by dashed lines). GA also appears to even out the "polarity gradient" along the lipid chain. This effect is most evident for 16-PC where the addition of GA decreases the g_{xx} value by 5.7×10^{-4}, corresponding to a shift of about 25 G in the 250-GHz spectrum! In pure DPPC samples, significant broadening is also observed for *n*-PC spin labels in the 9-GHz spectra (cf. Fig. 5). It is difficult to distinguish the broad background signal in the 9-GHz spectra, but the addition of GA does significantly reduce the overall broadening of these spectra consistent with the loss of a broad background signal.

We were not able to fit the background feature quantitatively with either a model of HE, or by subtracting out a broad Gaussian or Lorentzian line. Nevertheless, by including a

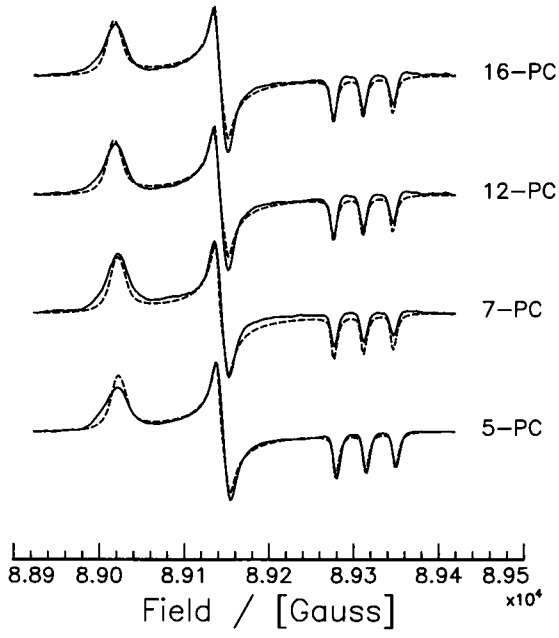

FIGURE 2 Rigid limit spectra of 5-, 7-, 12-, and 16-PC in DPPC (hydrated) with GA. The samples are ordered from bottom to top: 5-, 7-, 12-, and 16-PC. Note how the presence of GA strongly suppresses the background that is a major component in the rigid limit spectra of 7-, 10-, and 12-PC shown in Fig. 1. Spectral simulations are shown by a dashed line. The magnetic tensor parameters derived from the fits are given in Table 1.

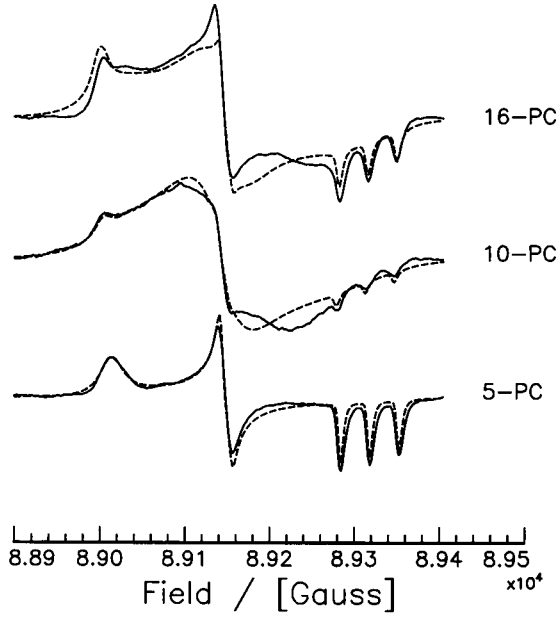

FIGURE 3 Rigid limit spectra of 5-, 10-, and 16-PC in POPC (hydrated). Spectra are plotted in order from bottom to top: 5-PC, 10-PC, and 16-PC. Best-fit simulations are shown as dashed lines. The magnetic tensor parameters derived from the fits are given in Table 2.

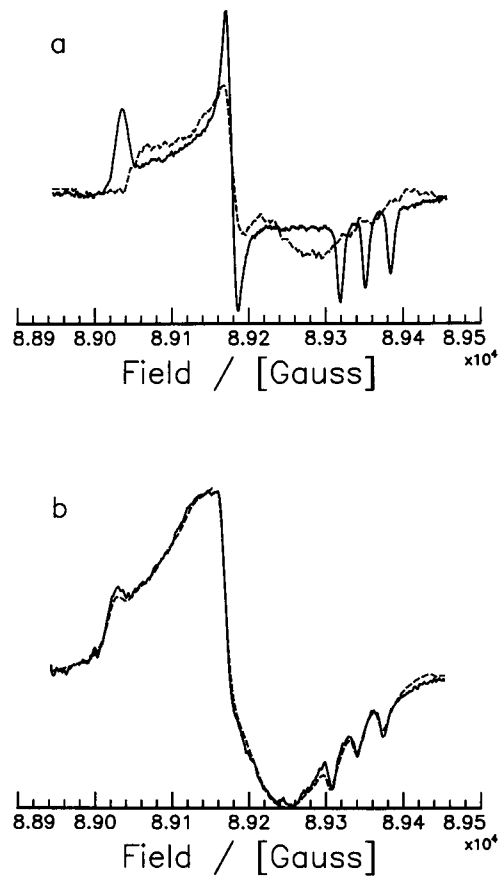

FIGURE 4 (*a*) 16-PC/DPPC at −150°C (*solid line*) and +5°C (*dashed line*). (*b*) 12-PC/DPPC spectra at two concentrations, 0.5 mol % (*solid line*) and 1.0 mol % (*dashed line*). Note that the shape of the background signal is independent of concentration for the 12-PC/DPPC spectra, and is still present in 16-PC/DPPC at 5°C.

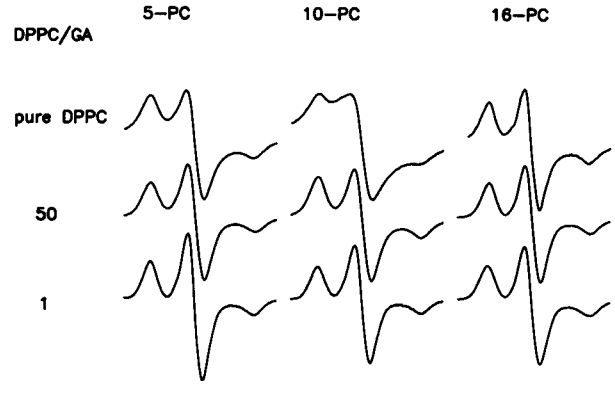

FIGURE 5 Rigid limit 9-GHz spectra of 5-, 10-, and 16-PC in DPPC (hydrated) with or without GA. The effect of adding GA to lipid dispersions is shown. The numbers in the left-most column indicate the ratio of DPPC to GA. Note that the background signal is strongly reduced when the concentration of GA is >0.02 mol % (Ge and Freed, 1993).

broad second component, which is assumed to be HE narrowed, we did reduce the root-mean-square deviation of the fit significantly, with the result that we could fit the magnetic tensor parameters with the uncertainties stated in Tables 1 and 2.

The overall agreement between the data and the spectral fit is not perfect; however, the discrepancy between the experimental background component and its simulation is only appreciable in the spectral region between g_{yy} and g_{zz}, as

TABLE 1 Magnetic tensor parameters of 5-, 7-, 12- and 16-PC spin probes in pure DPPC including the percentage of the exchange-narrowed site and DPPC/gramicidin A mixtures in a molar ratio of 1:1.

n-PC	g_X*	g_Y*	g_Z‡	A_X§	A_Y§	A_Z¶	%‖**
DPPC							
5	2.00869	2.00593	2.00212	4.9	4.9	35.0	18
7	2.00873	2.00594	2.00212	4.9	4.9	34.5	77
12	2.00880	2.00593	2.00212	4.9	4.9	34.0	72
16	2.00929	2.00600	2.00212	4.9	4.9	33.5	21
GA:DPPC							
5	2.00870	2.00593	2.00212	4.9	4.9	35.2	0
7	2.00868	2.00591	2.00212	4.9	4.9	35.1	0
12	2.00875	2.00591	2.00212	4.9	4.9	35.0	0
16	2.00867	2.00591	2.00212	4.9	4.9	35.1	0

* The relative error in this parameter is $\pm 2 \times 10^{-5}$.
‡ This parameter was not varied due to its small effect on the fitting procedure.
§ This parameter was not varied due to its poor resolution; parameter reported in Gauss.
¶ The uncertainty in this parameter is ±0.2 G; parameter reported in Gauss.
‖ This is the percent of exchange-narrowed component determined by a separate linear least squares fit to the experimental spectrum. The uncertainty is estimated to be +3%.
** For 10-PC/DPPC (not shown), we observed only a single exchange-narrowed line.

TABLE 2 Magnetic tensor parameters of 5-, 10-, and 16-PC spin probes in pure POPC including the percentage of the exchange-narrowed site

n-PC	g_X*	g_Y*	g_Z‡	A_X§	A_Y§	A_Z¶	%‖
5	2.00902	2.00597	2.00212	4.9	4.9	34.5	0
10	2.00910	2.00594	2.00212	4.9	4.9	34.2	92
16	2.00926	2.00593	2.00212	4.9	4.9	34.1	67

* The relative error in this parameter is $\pm 2 \times 10^{-5}$.
‡ This parameter was not varied due to its small effect on the fitting procedure.
§ This parameter was not varied due to its poor resolution; parameter reported in Gauss.
¶ The uncertainty in this parameter is ±0.2 G; parameter reported in Gauss.
‖ This is the percent of exchange-narrowed component (see note ‖, Table 1); 5-PC/POPC did not require an exchanging site.

shown in Figs. 1 and 3. This did not have a deleterious effect on determining the magnetic tensor parameters, because the discrepancy between the data and the simulation was minimal at the canonical turning points of the spectrum. Hence, even though the background component is not particularly well-fit, there is still enough spectral weight from the rigid limit component to ensure that g_{xx}, g_{yy}, and A_{zz} are well-determined parameters for all dispersions except 10-PC/DPPC. We have observed (Budil et al., 1989; Earle et al., 1993) that g_{zz} does not change appreciably for a variety of nitroxides in different environments, as expected from theory (Stone, 1962). We found it convenient in fitting the *n*-PC/DPPC dispersion spectra to vary g_{xx}, g_{yy}, Tr{g}, A_{zz}, and ω_{HE}, the Heisenberg exchange rate of the background component. The fraction of spins in the broad component was also determined by least squares fitting and varied as shown in Tables 1 and 2. The best fit value for the HE rate varied from 3 to 5 $\times$ 10^8 s^{-1}, and was not strongly sample-dependent.

We also fit these spectra with orientation-dependent broadening. Initial simulations showed that the spectra exhibited little variation of these widths as a function of position of the label on the chain or of sample composition. For convenience in fitting we utilized a single set of 'optimum' Lorentzian widths, determined from initial fits, in our final fits. They are $T_{2,ii}^{-1}/\gamma_e$ equal 7.5, 4, and 3.5 G for $i = x, y, z$, respectively. These results show the expected trends, with the largest *g*-strain associated with g_{xx} (Budil et al., 1989).

It is clear from this least squares procedure that the need to fit the rigid-limit spectra to two sites poses an additional challenge to the fitting, as noted in the introduction. Another factor is the substantial broadening we observe in the these spectra. Both features reduce the spectral resolution. In previous 250-GHz ESR studies on model systems of nitroxides, better overall resolution was observed. For a perdeuterated spin probe, PD-tempone (2,2′,6,6′-tetramethyl-4-piperidone) in perdeuterated toluene, the spectrum is sharp enough that we could achieve a relative error of $\pm 5 \times 10^{-6}$ in the *g*-tensor (Budil et al., 1993) (i.e., to within a factor of about 3 of the resolution of two infinitely sharp lines, see Experimental Methods), and for cholestane (3-doxyl cholestan-3-one) in toluene the somewhat broader lines led to a relative error of $\pm 7 \times 10^{-6}$. This is to be compared with our present relative error of $\pm 2 \times 10^{-5}$ as determined from the nonlinear least squares fits. Nevertheless, this degree of resolution is more than sufficient to accurately measure the changes in g_{xx} with location on the chain, type of lipid, or presence of GA.

It is also true that the resolution for the *g*-tensor for the systems studied in the present work is significantly improved at 250 GHz compared with 9 GHz. This is illustrated in Fig. 6 where we superpose in Fig. 6 *a* the 250-GHz spectra from 16- and 5-PC/DPPC and in Fig. 6 (*b*) the equivalent 9-GHz spectra. The large (27 G) spectral shift due to the difference in g_{xx} is very clear for the 250-GHz spectra as well as the smaller (1.5 G) difference in A_{zz}. On the other hand, any spectral shift due to differences in g_{xx} is hidden at 9 GHz in the broad central component (cf. Fig. 6 *b*). One predicts a 1-G shift which is buried in the central component composed of the main unexchanged spectrum with inhomogeneous broadening of T_2^{-1}/γ_e = 5 G, and the exchange-broadened spectrum. Together they yield an overall peak to peak width of the central component of about 10 G.

Despite the poor resolution, we performed nonlinear least squares fits to the 9-GHz spectra shown in Fig. 6 *b* to see to what extent the magnetic tensors could be recovered. We found that they could not be reliably recovered. Unlike the case for 250 GHz, their values depended significantly on precisely how the nonlinear least squares was performed (e.g., whether the fitting of the two components in the spectrum was performed in separate steps or concurrently). For example, g_{xx} could vary by as much as 1×10^{-3}, yet the fits to the 9-GHz spectra were of comparable quality (cf. Fig. 6, *c* and *d*). This difficulty in fitting the poorly resolved 9-GHz spectra can be attributed, to a large extent, to the large correlations that exist between the least squares parameters as shown by the correlation coefficients for typical cases (cf.

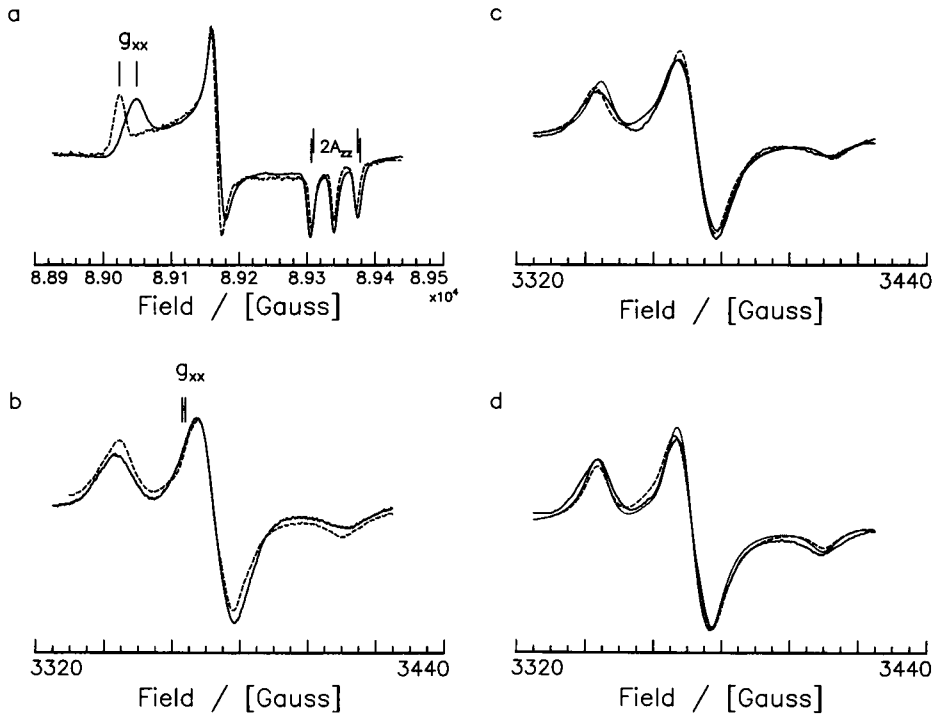

FIGURE 6 (*a*) Superposition of experimental 250-GHz spectra from 5-PC/DPPC (*solid line*) and 16-PC/DPPC (*dashed line*) showing the shifts in g_{xx} and A_{zz}. (*b*) Superposition of experimental 9-GHz spectra from 5-PC/DPPC (*solid line*) and 16-PC/DPPC (*dashed line*) showing location of the central g_{xx} position. (*c*) and (*d*) show 9-GHz spectra for 5- and 16-PC/DPPC, respectively. The experimental spectrum is shown by the solid line; the dashed line is the simulation based on the magnetic tensors given in Table 1; the dotted line is the result from a nonlinear least squares fit of the 9-GHz spectrum using the exact procedure followed in the fit to the 250-GHz spectra. Both sets of parameters yield virtually identical residuals for *c* and *d*. The best fit 9-GHz magnetic tensor parameters are $g_{xx} = 2.0103, g_{yy} = 2.0060, g_{zz} = 2.0021, A_{xx} = 4.9$ G, $A_{yy} = 4.9$ G, $A_{zz} = 34.0$ G for 5-PC/DPPC and $g_{xx} = 2.0091, g_{yy} = 2.0060, g_{zz} = 2.0021, A_{xx} = 4.9$ G, $A_{yy} = 4.9$ G, $A_{zz} = 33.5$ G for 16-PC/DPPC.

Table 3) versus those for the 250-GHz spectra (also in Table 3). These correlations emphasize the fact that the exchange-narrowed component in the central region has a deleterious effect, and to this we add the fact that our model does not reproduce this component especially well (which we could only determine from the much better resolved 250-GHz spectra).

For the better resolved case of PD-Tempone in deuterated toluene, referred to above, it was found that *g*-tensor components with $\pm 2 \times 10^{-4}$ relative error could be recovered at 9 GHz compared with the $\pm 5 \times 10^{-6}$ value at 250 GHz (Budil et al., 1993; Hwang et al., 1975). Thus, the reduced resolution for the case of the *n*-PC labels in membrane dispersions clearly has a more deleterious effect on the ability to resolve the *g*-tensor components at 9 GHz than at 250 GHz.

TABLE 3 A. Correlation matrices for 5-PC/DPPC, magnetic tensors as in Table 1. The 9-GHz parameters used are given in the legend to Fig. 6

	g_{XX}	g_{YY}	A_{ZZ}	ω_{HE}
	1.000	0.4832	0.1277	−0.0521
250 GHz		1.000	−0.1202	0.2335
			1.000	−0.5901
				1.000
	1.000	0.1085	−0.6520	0.7688
9 GHz		1.000	0.1426	0.0374
			1.000	−0.9409
				1.000

B. Correlation matrices for 16-PC/DPPC, magnetic tensors as in Table 1. The 9-GHz parameters used are given in the legend to Fig. 6.

	g_{XX}	g_{YY}	A_{ZZ}	ω_{HE}
	1.000	0.4779	0.1095	−0.0059
250 GHz		1.000	−0.0445	0.1178
			1.000	−0.5420
				1.000
	1.000	0.0504	−0.6401	0.7795
9 GHz		1.000	0.1358	0.0506
			1.000	−0.9136
				1.000

DISCUSSION

We were able to determine the magnetic tensor parameters for all dispersions studied, except for 10-PC/DPPC. This allowed us to examine the effect of the chain position of the spin label on the rigid limit magnetic tensor parameters of *n*-PC in DPPC, POPC, and GA:DPPC dispersions, cf. Fig. 7. We make the following observations: (1) In *n*-PC/DPPC dispersions g_{xx} increases monotonically but nonlinearly and A_{zz} decreases linearly with *n*; (2) for *n*-PC/POPC dispersions, g_{xx} and A_{zz} are linearly correlated; (3) the *n*-PC/GA:DPPC dispersions have g_{xx} and A_{zz} values essentially independent of *n*.

The significant variation of g_{xx} and A_{zz} with label position in pure lipid dispersions most likely results from changes in the polarity of the local environment sampled by the spin label at different positions along the lipid chain. The most natural explanation for such a change is that the penetration of water is increasingly hindered as it tries to proceed further down the hydrophobic alkyl chain. The observation that g_{xx} increases on going from the polar headgroup to the hydrophobic region is consistent with previous high-field results from our laboratory for the PDT spin probe in solvents of differing polarity (Budil et al., 1989). For example, we have found in the past that g_{xx} of PDT is 2.00853 in the polar glycerol/water solvent, but 2.00963 in the much less polar

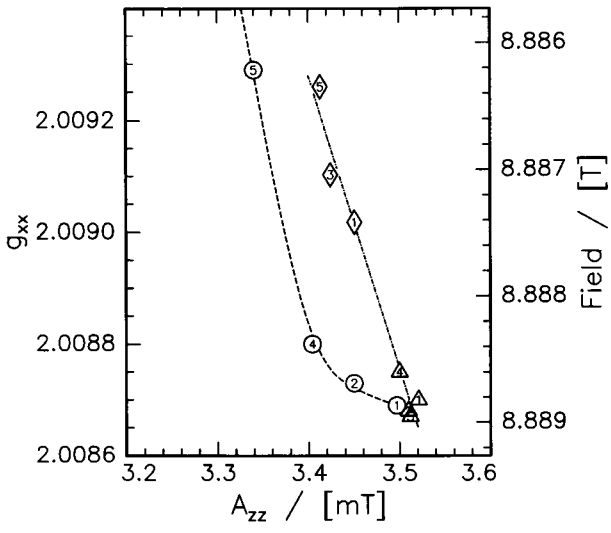

FIGURE 7 Graph of g_{xx} versus A_{zz}. The magnetic tensor parameters g_{xx} and A_{zz} (in units of mT) are plotted. (○) 'pure' DPPC dispersions; (△) GA/DPPC dispersions; (◇) POPC dispersions. The numbers correspond to the *n*-PC labels studied: 1 ⇒ 5-PC, 2 ⇒ 7-PC, 3 ⇒ 10-PC, 4 ⇒ 12-PC, 5 ⇒ 16-PC.

toluene solvent. This trend is also consistent with that found by Lebedev and co-workers in 140-GHz studies of solvent effects (Krinichnyi et al., 1984; 1985) and structural effects (Ondar et al., 1985a) on nitroxide spin labels.

One might speculate that nonideal mixing of the *n*-PC labels may be playing a role in the significant increase of overall water penetration into the membrane. However, this does not seem to be the case, because it would predict that the effects on g_{xx} and A_{zz} should be maximized when the exchange-narrowed spectral component is largest (e.g., for 10-PC/POPC), which is in disagreement with our observations (cf. Tables 1 and 2). Our results would be consistent with a model in which the aggregates of spin-labeled lipids contributing to the exchange-narrowed line are entities that are distinct from the vesicles which include magnetically diluted spin-labeled lipids that contribute to the well-resolved spectral component.

The results in Fig. 7 are divided into two classes: those systems that show a linear increase of g_{xx} as A_{zz} decreases, such as the *n*-PC/POPC and *n*-PC/GA:DPPC data; versus the *n*-PC/DPPC data, which show a nonlinear trend. Previous work (Kawamura et al., 1967) has shown that nitroxide spin labels can have different *g* versus *A* dependences, depending on whether the local environment is protic or aprotic. Moreover, the data for protic solvents are described by a linear relation with a steeper slope than for aprotic solvents. A partial explanation of the effects that we observe may then be that the different lipid dispersions have qualitatively different polarity gradients. This would suggest that both the kink structure in POPC and the high concentration of GA in the *n*-PC/GA:DPPC dispersions promotes a protic environment for the *n*-PC spin labels. For the *n*-PC/DPPC dispersions, the gentler overall slope of the g_{xx} versus A_{zz} dependence is suggestive of an aprotic environment, which is consistent with a model of well-packed hydrophobic alkyl chains. However, this effect probably cannot entirely account for the pronounced curvature of the g_{xx} versus A_{zz} curve shown in Fig. 7 for DPPC.

The nonlinear dependence of g_{xx} on A_{zz} for *n*-PC/DPPC dispersions could be due to another effect. A previous study (Meirovitch and Freed, 1980) has found evidence suggesting that sterically induced strains in 7,6-PC, and 12-doxylstearic acid probes can affect the hyperfine tensor parameters. It is intriguing to speculate that sterically induced strains on the *n*-PC spin labels, particularly for 7-, 10-, and 12-PC/DPPC dispersions may cause departures from linearity of g_{xx} versus A_{zz}, as well as promote spin-label aggregation.

Previous work (Griffith et al., 1974) has demonstrated that the value of A_{zz} is significantly affected by hydrogen-bonding if the spin labels are in contact with water. That work also showed that water penetrates into the lipid bilayer of aqueous suspensions or hydrated samples. Moreover, spin labels at the C_{12} position and farther from the polar head group did not exhibit a strong dependence on the amount of water in the sample, which indicates that water penetration is frustrated beyond one-fourth of the width of the bilayer (Griffith et al., 1974).

Ondar et al. (1985b) have demonstrated in other systems that five-member ring nitroxide spin labels (such as the doxyl group in the *n*-PC labels) are particularly sensitive to the effects of hydrogen bonding. The effect is most pronounced for g_{xx}; in fact one may observe a distribution of g_{xx} values in the presence of hydrogen bonding. The slightly asymmetric appearance of the g_{xx} region of the spectra in Fig. 2 suggests that there is a distribution of g_{xx} values in GA-containing dispersions which may reflect hydrogen-bonding interactions with water. This distribution is not evident in A_{zz}. This is because the relatively large spectral shifts observed at high fields due to changes in g_{xx} correspond to small changes in A_{zz}, which are obscured by the linewidth (Ondar et al., 1985b).

Although we have not as yet performed extensive temperature-dependent studies of lipid dispersions by FIR-ESR, one must recognize that a detailed analysis of rigid limit tensor parameters is likely to only be a qualitative guide to the microenvironment of lipid dispersions at higher temperatures, particularly for high resolution methods such as FIR-ESR. One expects, and in fact observes (Krinichnyi et al., 1984) temperature-dependent magnetic tensor parameters. Upon warming up from the rigid limit, the polarity of the spin-probe microenvironment will change as the penetration of water into the lipid bilayer varies. Methods of accounting for magnetic tensor parameter variation are described elsewhere (Krinichnyi et al., 1984). We would like to note, however, that the enhanced *g*-resolution of FIR-ESR and the empirical relationship between changes in the *g*-tensor and the polarity of the local environment that we have determined in this work can be exploited to elucidate details of polarity effects within the lipid bilayer. Also FIR-ESR in combination with other techniques such as

pulsed-ESR and conventional CW-ESR at X-band (9.5 GHz) provide complementary information about spin-label dynamics, as we have demonstrated previously (Budil et al., 1993; Earle et al., 1993).

The lineshape and linewidth of the background signals shown in Fig. 1 are qualitatively similar to 250-GHz spectra of nitroxide spin probes undergoing slow reorientations (Earle et al., 1993), and would seem to reflect some type of dynamic averaging. Because the samples are in the rigid limit at −150°C, one can safely exclude rotational motion of the probe, but exchange interactions among the spin-labeled molecules are possible. We did examine the dependence of the background signal on the spin probe concentration of the 12-PC probe and the temperature dependence of the 16-PC probe; we found that the lineshape of the background is essentially independent of these variables (cf. Fig. 4). To resolve structure in the broad component, it would be necessary to go to high enough frequencies that the unexchanged spectral extent (determined by the g-tensor but measured in frequency units) would be much greater than the exchange rate. Measurements at lower microwave frequencies would not be expected to show any resolved structure.

The low spin label concentrations used (0.5–1.0 mol %) and the absence of any concentration dependence would also appear to rule out any significant HE or EED interactions in the sample, if the spin label is assumed to be distributed homogeneously. The amount of g-strain that would be required to reproduce the broad component is not physical for a homogeneous distribution of spins. However, appreciable spin-spin interactions would still be possible if the spin-labeled molecules are aggregated into clusters in the dispersion due to nonideal mixing of the probe with the host lipid. Such nonideality could arise from the bend in the lipid chain introduced by the doxyl ring of the spin label, which inhibits close packing of the probe molecule with the saturated chains of DPPC in the gel phase. This model is consistent with the rather unusual dependence of the background signal on chain label position: when the bend is introduced in the middle of the chain, as for 10-PC, it is most effective in preventing chain packing, whereas the packing of end-labeled lipids is much less perturbed by the bend. These conclusions are consistent with results from 9-GHz saturation-transfer ESR studies of Fajer et al. (1992), who found significant spin-spin interactions among n-PC spin labels in the low-temperature phases of DPPC, and also found that the spin-spin interactions are greatest when the spin label is located near the center of the chain.

Our study of 5-, 10-, and 16-PC/POPC dispersions enabled us to test the effects of chain packing on the observed spin-spin interactions. POPC has a bend at the C_9 position of the sn-2 chain resulting from an unsaturated bond. It is, therefore, sterically more similar to n-PC probes and should exhibit more ideal mixing with them, especially with 10-PC. The broad background was still very apparent as one may see from Fig. 3. However, for 10-PC we find that the intensity of the broad signal is significantly reduced and the overall linewidth increased in POPC relative to that in 16-PC/POPC. This result supports the idea that the broad signal is related to nonideal mixing interactions, or packing effects. It should be noted that despite steric symmetry, the bulky doxyl ring may prevent the mixing from being ideal even for POPC because the kink structure is different for 10-PC and POPC.

We find that the addition of GA to the DPPC dispersion at a molar ratio of 1:1 almost completely abolishes the broad background signal. GA also appears to even out the "polarity gradient" along the lipid chain, because the values of g_{xx} and A_{zz} that we observe are clustered around similar values as shown in Fig. 7. It is important to note that the effect of GA on the DPPC dispersions is so large because the environment sampled by the n-PC/DPPC mixtures at the 1:1 molar ratio used in this work is no longer a lipid bilayer. From steric considerations, it is clear that the volume fraction of the peptide dominates the dispersion. The lipid, spin label, and water molecules should thus be seen as squeezed between large GA aggregates. This either promotes uniform exposure of the alkyl chains of the lipid to water, or, alternatively, to an electrostatic interaction with the GA, perhaps via a hydrogen-bonding interaction with an amino side chain of the peptide (e.g., tyrosine) or with the dipole moment of the peptide's α-helical structure. Such a model would explain why water penetrates more easily in GA/DPPC dispersions, and also why the magnetic tensor parameters that one observes are more typical of a polar environment.

CONCLUSIONS

Rigid limit spectra from the n-PC series of spin labels in DPPC dispersions exhibit great sensitivity to the position of the doxyl label, particularly for the g_{xx} and A_{zz} magnetic tensor components. The spectral changes as a function of label position are attributed to differences in the polarity of the local environment due to different degrees of water penetration along the hydrophobic alkyl chains of the membrane bilayer. The spectra from n-PC/POPC dispersions show a less dramatic dependence on the label position. This may be due to the kink at the unsaturated C_9 position of the sn-2 chain, which can allow greater water penetration into POPC membranes.

When GA is included into the DPPC dispersions in a 1:1 molar ratio, g_{xx} and A_{zz} for the n-PC series cluster around values characteristic of a polar environment, independent of the label position. One explanation of this behavior is that the presence of GA disrupts the local membrane structure, possibly by formation of GA aggregates, so that water has uniform access to the hydrocarbon chains of the lipids.

Both n-PC/DPPC and n-PC/POPC dispersions exhibit a characteristic broad background signal that is most pronounced for spin labels near the middle of the alkyl chain. This effect is attributed to spin-label aggregation, which may result from nonideal mixing with the host lipid due to steric effects of the doxyl ring on the alkyl chain. The effect is less pronounced in POPC membranes, suggesting that POPC mixes better with the spin labels because of the bend at the unsaturation in the sn-2 chain. The background signals are

not well-fit by a simple model of Heisenberg spin exchange; however, the fits might be improved by including electron-electron dipolar interactions, or by including a distribution of exchange rates.

The results clearly show the value of the enhanced g-tensor resolution of 250-GHz ESR for studying both structural and dynamic effects in membranes, and in particular demonstrate its sensitivity as a tool for probing changes in local polarity, water penetration, and molecular clustering effects in lipid bilayers.

This research was supported by National Institutes of Health grants GM25862 and RR07126, and National Science Foundation grant CHE9312167. J.K.M. acknowledges partial support by KBN grant PB20889101, and D.E.B. acknowledges support through National Institutes of Health National Research Service Award GM-12924. Computations were performed at the Cornell National Supercomputer Facility (CNSF). We thank David Schneider of the CNSF for useful discussions, Dr. Alexander Wood of Ithaca Cayuga Optical Services for his gift of polishing materials, which facilitated the construction of the Fabry Perot resonator used in this work, and Curt Dunnam of the Cornell Electron Storage Ring (CESR) support staff for his development of the transconductance amplifier used to drive the modulation coils of the FIR-ESR spectrometer.

REFERENCES

Broido, M. S., I. Belsky, and E. Meirovitch. 1982. Comparative study of the electron spin resonance behavior of doxyl-labeled and (minimum steric perturbation) azethoxyl-labeled fatty acids in several liquid crystalline mesophases. *J. Phys. Chem.* 86:4197–4205.

Budil, D. E., K. A. Earle, and J. H. Freed. 1993. Full determination of the rotational diffusion tensor by electron paramagnetic resonance at 250 GHz. *J. Phys. Chem.* 97:1294–1303.

Budil, D. E., K. A. Earle, W. B. Lynch, and J. H. Freed. 1989. Electron paramagnetic resonance at 1 millimeter wavelengths. *In* Advanced EPR: Applications in Biology and Biochemistry. Elsevier, Amsterdam. 307–340.

Burghaus, O., A. Toth-Kischkat, R. Klette, and K. Moebius. 1988. Proton ENDOR at a microwave frequency of 97 GHz. *J. Magn. Res.* 80:383–388.

Earle, K. A., D. E. Budil, and J. H. Freed. 1993. 250 GHz EPR of nitroxides in the slow-motional regime: models of rotational diffusion. *J. Phys. Chem.* 97:13289–13297.

Fajer P., A. Watts, and D. Marsh. 1992. Saturation transfer, continuous wave saturation, and saturation recovery electron spin resonance studies of chain-spin labeled phosphatidylcholines in the low temperature phases of dipalmitoyl phosphatidyl-choline bilayers. *Biophys. J.* 61:879–891.

Freed, J. H. 1993. Notes on Heisenberg exchange in the slow motional limit. Cornell University, Ithaca, NY. (to be published)

Ge, M., and J. H. Freed. 1993. An ESR study of interactions between gramicidin A′ and phosphatidylcholine bilayers. *Biophys. J.* 65: 2106–2123.

Golub, G. H., and V. Pereyra. 1973. The differentiation of pseudo-inverses and nonlinear least squares problems whose variables separate. *SIAM (Soc. Ind. Appl. Math.) J. Num. Anal.* 10:413–432.

Griffith, O. H., P. J. Dehlinger, and S. P. Van. 1974. Shape of the hydrophobic barrier of phospholipid bilayers (evidence for water penetration in biological membranes). *J. Membr. Biol.* 15:159–192.

Grinberg, O. Y., A. A. Dubinskii, and Y. S. Lebedev. 1983. Electron paramagnetic resonance of free radicals in the two-millimeter wavelength range. *Russian Chem. Rev.* 52:850–865.

Hwang, J. S., R. P. Mason, L.-P. Hwang, and J. H. Freed. 1975. Electron spin resonance studies of anisotropic rotational reorientation and slow tumbling in liquid and frozen media. III. Perdeuterated 2,2′,6,6′-tetramethyl-4-piperidone *N*-oxide and an analysis of fluctuating torques. *J. Phys. Chem.* 79:489–511.

Hyde, J. S., H. M. Swartz, and W. E. Antholine. 1979. The spin-probe–spin-label method. *In* Spin-Labeling II, Theory and Applications. L. J. Berliner, editor. Academic Press, New York. 71–114.

Jost, P. C., and O. H. Griffith. 1982. Lipid-Protein Interactions. John Wiley & Sons, New York.

Kar, L., G. L. Millhauser, and J. H. Freed. 1984. Detection of slow motions in oriented multilayers by two-dimensional electron-spin-echo spectroscopy. *J. Phys. Chem.* 88:3951–3956.

Kawamura, T., S. Matsunami, and T. Yonezawa. 1967. Solvent effects on the g-value of di-*t*-butyl nitric oxide. *Bull. Chem. Soc. Jpn.* 40:1111–1115.

Krinichnyi, V. I., O. Y. Grinberg, V. R. Bogatyrenko, G. I. Likhtenstein, and Y. S. Lebedev. 1985. Study of microenvironment effect on magnetic resonance parameters of spin-labeled human serum albumin in 2 mm ESR range. *Biofizika.* 30:216–219.

Krinichnyi, V. I., O. Y. Grinberg, E. I. Yudanova, E. V. Lyubashevskaya, L. I. Antsiferova, G. I. Likhtenstein, and Ya. S. Lebedev. 1984. Study of lysozyme by spin label in two-millimeter range. *Biofizika.* 32:215–220.

Lynch, W. B., K. A. Earle, and J. H. Freed. 1988. A 1 millimeter-wave ESR spectrometer. *Rev. Sci. Instrum.* 59:1345–1351.

Marsh, D. 1985. *In* Progress in Protein-Lipid Interactions. Amsterdam, Elsevier. 143–172.

Marsh, D. 1989. Experimental Methods in Spin-Label Spectral Analysis. *In* Spin Labeling: Theory and Applications. Plenum Press, New York. 255–337.

Meirovitch, E., and J. H. Freed. 1980. ESR studies of low water content 1,2-dipalmitoyl-*sn*-glycero-3-phosphocholine in oriented multilayers. 1. Evidence for long-range cooperative chain distortions. *J. Phys. Chem.* 84:3281–3295.

Moré, J. J., B. S. Garbow, and K. E. Hillstrom. 1980. User's Guide for MINPACK-1. National Technical Information Service, Springfield, VA.

Muller, F., M. A. Hopkins, N. Coron, M. Grynberg, L. C. Brunel, and G. Martinez. 1989. A high field EPR spectrometer. *Rev. Sci. Instrum.* 60: 3681–3684.

Ondar, M. A., O. Y. Grinberg, A. A. Dubinskii, A. F. Shestakov, and Y. S. Lebedev. 1985a. ESR spectroscopy in the two-millimeter band and magnetic resonance parameters. *Sov. J. Chem. Phys.* 2:83–92.

Ondar, M. A., O. Y. Grinberg, A. A. Dubinskii, and Ya. S. Lebedev. 1985b. Study of the effect of the medium on the magnetic-resonance parameters of nitroxyl radicals by high-resolution EPR spectroscopy. *Sov. J. Chem. Phys.* 3:781–792.

Prisner, T. F., S. Un, and R. G. Griffin. 1992. Pulsed ESR at 140 GHz. *Isr. J. Chem.* 32:357–363.

Schneider, D. J., and J. H. Freed. 1989. Spin relaxation and molecular dynamics. *Adv. Chem. Phys.* 73:387–528.

Shin, Y. K., and J. H. Freed. 1989. Thermodynamics of phosphatidylcholine-cholesterol mixed model membranes in the liquid crystalline state studied by the orientational order parameter. *Biophys. J.* 56:1093–1100.

Stone, A. J. 1962. g factors of aromatic free radicals. *Mol. Phys.* 1963: 509–515.

Tanaka, H., and J. H. Freed. 1985. Electron spin resonance studies of lipid-gramicidin interactions utilizing oriented multibilayers. *J. Phys. Chem.* 89:350–360.